

# **Multi-proxy record of Holocene Paleohydrology from alpine lake sediment on the Wasatch Plateau of central Utah, USA**

**Lesleigh Anderson<sup>\*1</sup>, Gary Skipp<sup>1</sup>, Laura Strickland<sup>1</sup>, Jeff Honke<sup>1</sup>, Jeremey Havens<sup>1</sup>, Paco VanSistine<sup>1</sup>**

<sup>1</sup>U.S. Geological Survey Geoscience and Environmental Change Science Center, Denver CO

\*Corresponding author, Lesleigh Anderson (land@usgs.gov)

\_\_\_\_\_ USGS Disclaimer for draft versions (not for publication) \_\_\_\_\_

This draft manuscript is distributed solely for purposes of scientific peer review. Its content is deliberative and pre-decisional, so it must not be disclosed or released by reviewers. Because the manuscript has not yet been approved for publication by the U.S. Geological Survey (USGS), it does not represent any official USGS finding or policy.

**Keywords:** Holocene, paleohydrology, lake level, carbonate oxygen isotopes, Upper Colorado, high elevation lake, Great Basin

## **Abstract**

The Holocene sediments at 3090 m elevation in Emerald Lake, central Utah, document the paleohydroclimatic history of the western Upper Colorado headwater region. Multi-proxy analyses of sediment composition, mineralogy, and stable isotopes of carbonate ( $\delta^{18}\text{O}$ ) shows changes in precipitation minus evaporation (P-E) for the past ~10,000 cal yr BP (calibrated year before present as 1950) at millennial to decadal timescales. Emerald Lake originated as a shallow closed-basin cirque pond during the early Holocene. Higher P-E and rising lake levels by ~7000 cal yr BP initiated littoral carbonate sedimentation near modern lake configurations and relatively high  $\delta^{18}\text{O}$  values indicate increased proportions of summer precipitation that continued until ~5500 cal yr BP when a landslide moved into the lake. Between ~4500 and 2400 cal yr BP dry conditions at Emerald Lake envelop the timing of the ‘Late Holocene Dry Period’ identified at low valley elevations. For the past ~2500 years, Emerald lake- $\delta^{18}\text{O}$  values were relatively low, indicating higher snow (relative to rain) except for dry periods at ca. 2000 cal yr BP and during the Medieval Climate Anomaly. Results show that precipitation extremes in the intermountain region similarly present at high and low elevation sites, are commonly regional and include precipitation dipoles and time-transgressive precipitation patterns. The high elevation Emerald Lake record further elucidates long-term perspectives on regional water supply and broadens the context for evaluating variations in snowpack for the observational period and its future prognosis.

## **Introduction**

Historic droughts in the intermountain region of the Rocky Mountains, including the Upper Colorado River basin (UCB), are compounded by reductions in snowpack, which is the

region's primary water source, and highlights the need for Holocene perspectives on precipitation extremes and drought (defined as meteorological drought, e.g., Mishra and Singh, 2010). In the continental interior of the American west, the seasonal interplay between atmospheric flow patterns (i.e., the jet stream) with geographic mechanisms and topography leads to winter maxima in the annual distribution of precipitation and higher precipitation amounts with elevation (Bryson and Hare, 1974; Redmond, 2003; Shinker et al., 2006; Shinker and Bartlein, 2011). Mountain snowpack is of fundamental importance for water supply because it contributes most of the water for storage and use at low elevations. Low elevation locations, including pluvial lakes, constitute the majority of the late Pleistocene records that provide the framework for our current understanding of the paleohydrologic history of the region (Bartlein et al., 1998; Madsen et al., 2001; McGee et al., 2012; Oviatt, 2015; Thompson et al., 2016, 1993).

Low valley elevations have relatively warm temperatures and lower annual precipitation amounts and semi-aridity frequently characterizes most of a year, and can lead to unique proxy sensitivity to wet and dry conditions by comparison with nearby alpine areas (Munroe and Laabs, 2020; Quirk et al., 2020; Wahl et al., 2015). Redmond (2006) identified the complex relationship between lower elevation surface water amounts and mountain snowpack by recognizing that peak snowmelt during spring runoff is brief, and commonly occurs before peak ecological water use during summer growing seasons when rainfall is infrequent and sporadic. There is an important distinction between the paleohydrology of high elevation locations where most water is supplied versus low elevations locations where most water is used. Records of regional water supply can be found at high elevation snowfall dominated locations with a precipitation sensitivity proxy, which in the case is water isotope tracers from lakes and their hydrologic budgets.

Lakes are natural reservoirs of mixed surface and meteoric waters and stable isotope ratios are widely used to study hydrologic and hydroclimatic processes, past and present (Gibson et al., 2016; Horton et al., 2016). Lake water isotopes of oxygen and hydrogen,  $\delta^{18}\text{O}$  and  $\delta^2\text{H}$  respectively, reflect processes related to water source and evaporation. Source waters reflect the isotope values of precipitation, including that which falls directly on a lake's surface combined with surface and groundwater inflow (Shapley et al., 2008). These are, in turn, related to the isotope effects of precipitation amount, atmospheric vapor source and trajectory and the temperature of condensation (Friedman, 2002a, 2002b; Smith, 2002). Evaporation from a lake's surface causes preferential loss of the light isotope  $^{16}\text{O}$ , which leads to a corresponding increase in the heavy isotope  $^{18}\text{O}$ , and thus higher  $\delta^{18}\text{O}$  values in the remaining lake water. There is greater potential for evaporation with extended lake water residence times, which is a function of lake hydrology that can be characterized by modern water isotope values (Smith and Palmer, 2012). A range of modern lake water isotope values provide helpful frameworks for the interpretation of past lake water isotope variations from sediment records such as those derived from lake carbonates (Anderson et al., 2016a).

Most existing lake carbonate  $\delta^{18}\text{O}$  records of the intermountain west are currently from low-elevation environments, including Walker and Pyramid Lakes in Nevada (Benson et al., 2002; Lund et al., 2021), Owens Lake and Mono Lakes in California (Li et al., 1997; Menking et al., 1997), and Bear Lake, Idaho-Utah (Bright et al., 2006; Dean et al., 2007). Holocene studies include Foy, Jones and Crevice Lakes in Montana (Shapley et al., 2009; Stevens et al., 2006; Stevens and Dean, 2008; Whitlock et al., 2013), San Luis Lake, in central Colorado (Yuan et al., 2013), and Lake Pahrnagat, in southern Nevada (Theissen et al., 2019). High elevation lake records are relatively uncommon in Utah (Munroe and Laabs, 2020) and those focused on

carbonate  $\delta^{18}\text{O}$  are currently limited to northwestern Colorado at Bison and Yellow Lakes, 3255 and 3140 m elevation respectively (Anderson, 2012, 2011). Located in the eastern Upper Colorado River Basin (UCB), the Bison and Yellow records characterize precipitation at multidecadal-scale resolution to provide regional Holocene snowpack trends (Anderson et al., 2016b). Additional high elevation carbonate  $\delta^{18}\text{O}$  records are needed evaluate patterns and processes related to seasonal precipitation, temperature, evapotranspiration, infiltration, and runoff across the sub-regions of the area that have yet to be explored by paleoclimatic investigations.

The objective of this study is to present a new lake carbonate  $\delta^{18}\text{O}$  paleoclimate record from Emerald Lake in central Utah, at 3090 m elevation (Fig. 1). The headwater lake is on the summit of the Wasatch Plateau, which delineates the border between the Great Basin and Colorado Plateau regions. The location of Emerald Lake in a previously undocumented on the western boundary of the UCB also provides a new opportunity to evaluate sub-regional snow and drought patterns within the watershed. The multi-decadal scale  $\delta^{18}\text{O}$  record (~30-year average resolution) is shown to sensitively records changes in precipitation and evaporation by utilizing a modern lake  $\delta^{18}\text{O}$  interpretive framework and sedimentary evidence for changes in lake level. Comparison with records from the eastern Great Basin and Northern Rockies approximates the geographic scale of synoptic climate patterns related to jet stream and North American Monsoon (hereafter ‘monsoon’) dynamics. Some of the questions to be addressed include: Were Holocene paleohydrologic trends consistent at high and low elevations? Were paleohydrologic extremes in the Upper Colorado typically basin-wide or were sub-regional variations more common? Is there evidence for precipitation dipoles and/or time-transgressive precipitation patterns that bear resemblance to historic patterns? How common are non-analogue conditions?

The Wasatch Plateau has a long history of damaging landslides, including mass movement that has evidently altered the western margin of Emerald Lake (Fig. 2; Baum and Fleming, 1989; DeGraff, 1978; Fleming et al., 1988; McDonald and Giraud, 2015). The primary mechanism for historic slope instability is soil saturation caused by either high snowmelt runoff or intense rainfall events. Holocene landslides may have also been triggered by seismic activity on steep normal fault segments of the Wasatch fault that cross the plateau, including the Emerald Lake watershed, (DuRoss et al., 2016; Machette et al., 1991; Witkind et al., 2006). An additional purpose of this study is to investigate the Emerald Lake sedimentary record for evidence of the landslide into the lake, to use the radiocarbon-based chronology for establishing the timing of the event, and to evaluate its occurrence within the context of the paleoclimatic record.

## **Study Site**

Emerald Lake (39.0738 °N, 111.4977 °W, 3090 m a.s.l.) is a headwater of the North Fork of Muddy Creek, a tributary of the Dirty Devil, Fremont, and Upper Colorado Rivers (Fig. 2) in the U.S. Department of Agriculture (USDA) Manti-La Sal National Forest. Emerald is located within the early Paleogene Flagstaff Formation, a lacustrine deposited in the Sevier foreland basin that consists of limestones, mudstones, minor sandstones and evaporites (Bowen et al., 2008). The limestones are locally dolomitic. During the Pleistocene, the Wasatch Plateau was glaciated (Larson, 1996; Spieker and Billings, 1940; Witkind et al., 2006) and megafaunal remains discovered in glaciolacustrine sediments include Columbian mammoth, mastodon, short-faced bear, horse and bison (Gillette and Madsen, 1993, 1992; Miller, 1987).

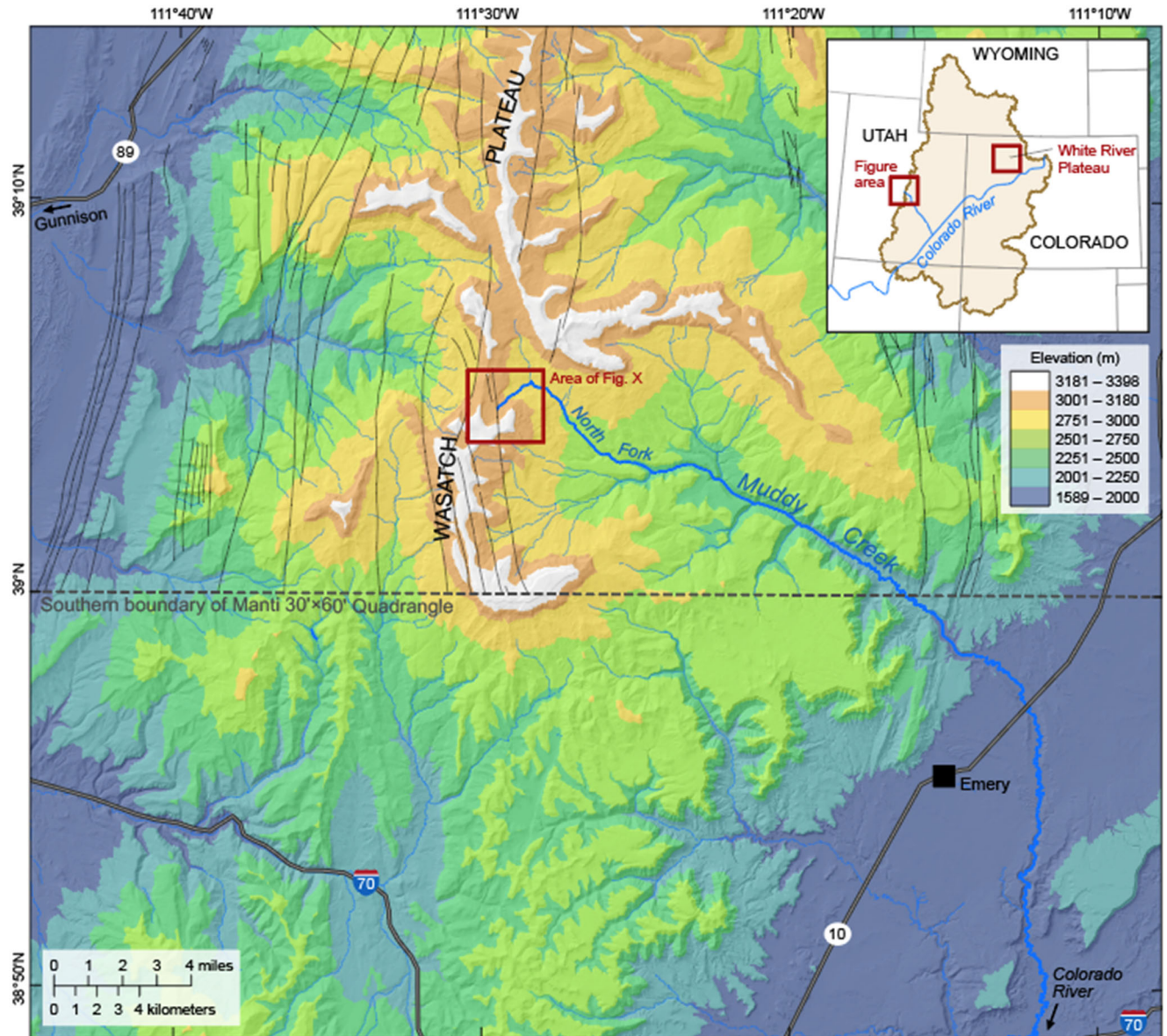


Figure 1: Map of the Emerald Lake study area (red box) within the Muddy Creek watershed in the southern Wasatch Plateau, central Utah on a colored digital elevation model. The inset shows the area's location in the Upper Colorado River Basin (UCB) in relation to the White River Plateau in northwest Colorado discussed in the text. North-south normal faults were mapped by Witkind et al. (2006) and are shown for the area of the U.S. Geological Survey Manti 30'x60' quadrangle.

The east side of the plateau crest is scalloped by glacial cirques, including the Emerald Lake basin, and that the primary source of ice accumulation was wind-blown snow (e.g.,

Dohrenwend, 1984). The Emerald cirque glaciers were ~2 km in extent and the lake is naturally impounded by a low ridge of Pleistocene till. It is primarily spring fed: a few minor ephemeral inflow streams occur and there is no surface outflow. A normal fault extends north-south across the Emerald Lake basin ~40 m lower than the lake surface where a spring outcrops. Whitkind et al (2006) mapped the fault which crosscuts the left and right lateral moraines to indicate that offsets were not observed. However, fault offset is clear where it intersects the west facing slopes of Block Mountain near a landslide front. On the north facing slope of Block Mountain a landslide post-date's the right-lateral moraine. If the landslides were triggered by fault movement, the fact that they crosscut the moraines may indicate post-glacial and Holocene seismic activity, such as those observed for Wasatch Fault segments to the north (DuRoss et al., 2016; Machette et al., 1991).

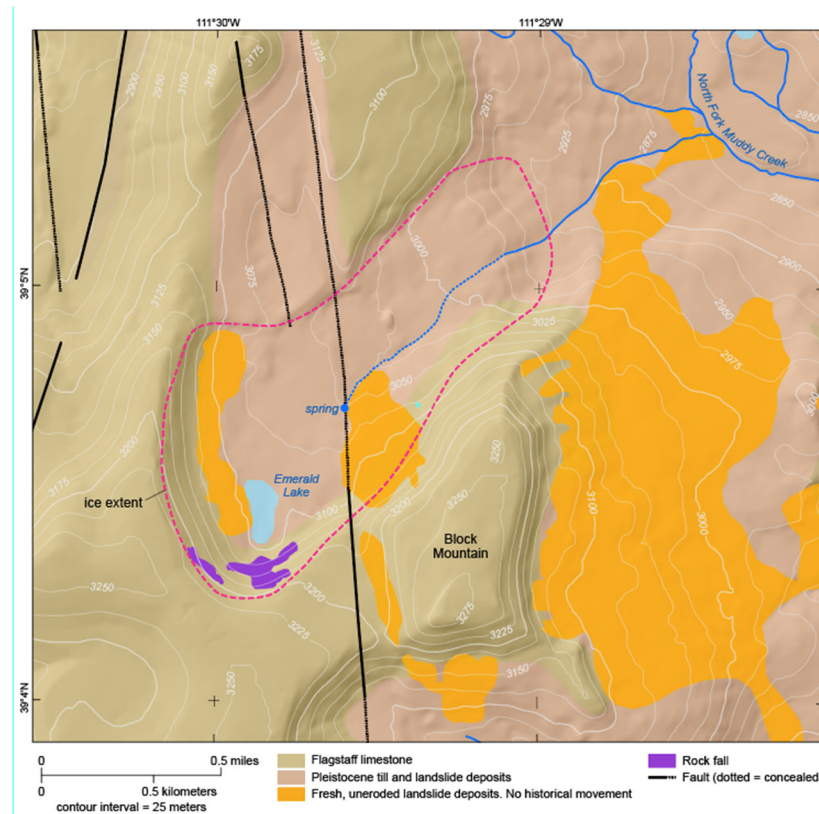




Figure 2: Expanded view of study area from Figure 1 of the Emerald Lake watershed with topography, faults, geologic units, landslides (orange) and rockfall (purple).

Emerald lake has a surface area of 0.032 km<sup>2</sup>, a watershed area of 0.412 km<sup>2</sup> (lake-to-watershed area ratio of 12), and a maximum depth of 8-m in a flat central area. Shallow littoral areas of < 2-m water depth occur along the southern margin and for portions of the western shoreline near the landslide front that moved down the east facing cirque (Fig. 3a). Where the landslide front is submerged, it slopes steeply downward to the lake's depocenter. Shallow margins to either side indicate that the landslide overran what was a continuous shallow area, thereby reducing the surface area of the lake (Fig 3b).

The sediments of Emerald Lake reflect the basin's watershed and limnology. The water column is thermally and chemically stratified during the summer and biologically mediated endogenic calcite precipitates within the alkaline and calcium saturated epilimnion. Thus, sediments at water depths within the epilimnion contain abundant well-preserved carbonates, but carbonate dissolution during settling within the water column limits the abundance at epilimnetic depths. Allochthonous sediments from the Flagstaff formation include mudstones, sandstones, calcite, and dolomite that were influenced by early Paleogene greenhouse climate on palustrine Flagstaff carbonate stable isotopes values in addition to paragenesis effects (Bowen et al., 2008). They differ isotopically from those of endogenic Holocene carbonates and allow assessment of the influence of detrital carbonate on the Holocene record, which is discussed in detail below.

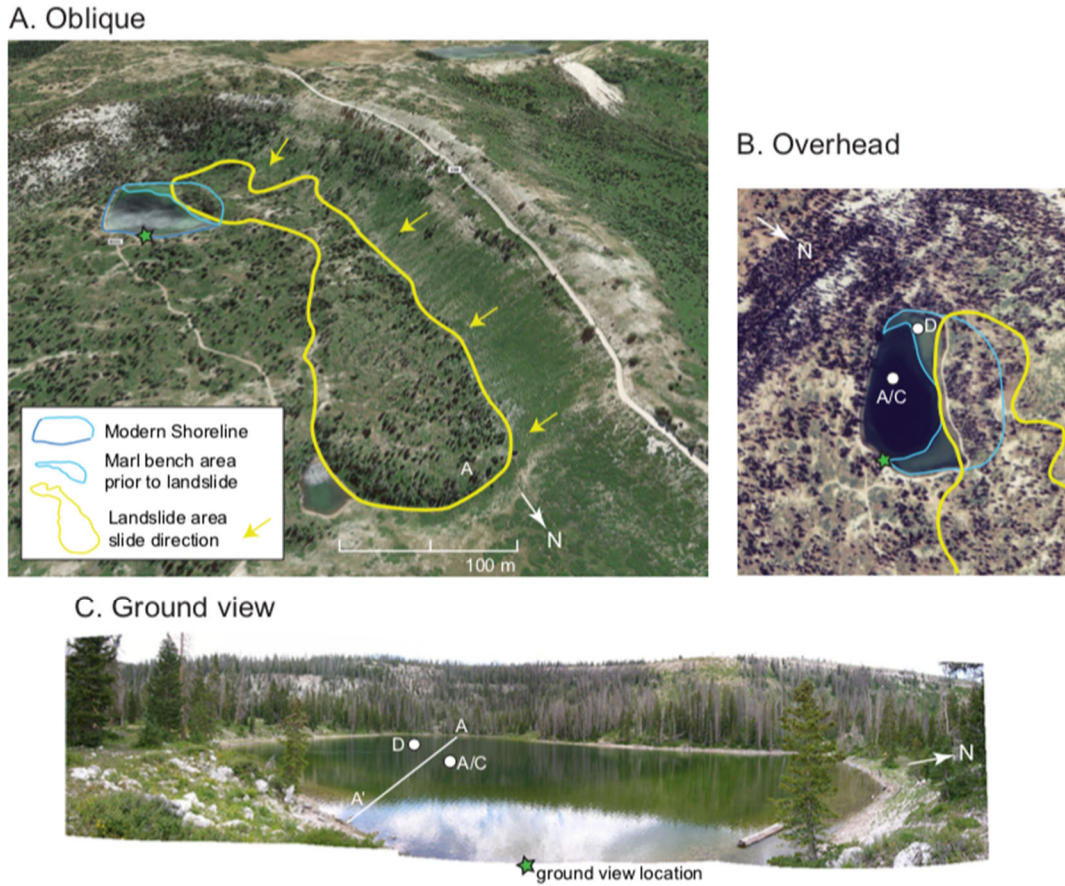


Figure 3: Emerald Lake imagery: A) an oblique view (Digital Globe), B) overhead (aerial photography) and C) ground view and core locations A/C and D (photo credit, Lesleigh Anderson). The modern shoreline in A is outlined in dark blue. The landslide into the lake is outlined in A and B in yellow and the inferred pre-landslide extent of the shallow marl bench is outlined in light blue. The location of the ground view is shown by a green star in A and C. The transect A-A' refers to the schematic block diagram in Figure 9.

Vegetation on the summit of the Wasatch Plateau is a mosaic of open grasslands, tundra, and fragmented stands of mature spruce and fir (*Picea Engelmannii* and *Pseudotsuga menziesii*, respectively) with lesser occurrence of ponderosa pine (*Pinus ponderosa*). Local ecosystem dynamics are driven by fire and insect outbreaks as well as weather extremes and herbivory. The extensive Engelman spruce mortality in the Emerald Lake watershed that is evident today (Fig. 3c) mostly occurred in 1986 and 1998 during a historic spruce beetle outbreak (*Dendroctonus*

*rufipennis*) which affected the entire Wasatch Plateau area (Dymerski et al., 2001). Previous severe disturbance of the landscape occurred during late 19<sup>th</sup> century high-grade logging (Morris et al., 2010) and dynamic fire regimes have influenced the landscape throughout the Holocene (Morris et al., 2015).

Climate of the Wasatch Plateau is significantly wetter and colder than elevations below 2000 m. For elevations >3000 m, the 30-yr climate normal are modeled by the Parameter-elevation Regressions on Independent Slopes Model (PRISM) and for mean annual precipitation are between 90 and 100 cm and for mean annual temperature are between -4 and -2°C (Oregon State University, 2018). The seasonal distribution of precipitation is strongly biased by winter, with snowfall accounting for ~70% of the annual total with monthly maximums in precipitation between February and April (Mock and Birkeland, 2000). Peak snowmelt runoff begins in early May and concludes by mid-to-late June. Snow water equivalent (swe) values in the Emerald Lake area range from 18 to 68 cm with a median of ~30 cm, based on data from the United States Department of Agriculture (USDA) National Resource Conservation Service (NRCS) high elevation snowpack telemetry (SNOTEL) Dill's Camp site (2795 m elevation, 1978 to present). For a snow-to-liquid ratio of 10:1, these swe values yield snowfall from ~2 to 7 m, although higher snow-to-liquid ratios and snow depths commonly occur. While summer precipitation may be associated with northern or western frontal boundaries, it most regularly occurs with intense convection associated with southerly upper level moisture that is usually associated with the monsoon (Adams and Comrie, 1997; Higgins et al., 1998).

## **Methods**

Emerald Lake sediment cores were retrieved in August 2006 from a securely anchored floating platform with a modified Livingstone piston corer at two sites 8-m and 1.45-m water depths, labeled core A/C and core D respectively. Deep water core A/C is a 270-cm length composite reported by Morris et al. (2015), which included analyses of macrofossils for radiocarbon, pollen, and charcoal. For this study, core A/C samples were obtained for dry bulk density and TC/TIC at continuous 1-cm increments ( $n = 296$ ). Percent organic and inorganic carbon was determined from dry, pulverized sub-samples using total carbon (TC) and total inorganic carbon (TIC) measurements by a UIC Inc. <sup>TM</sup> carbon dioxide coulometer (Engleman et al., 1985). Percent organic carbon was calculated as the difference between TC and TIC. The accuracy and precision for both TC and TIC is 0.1%.

Shallow water core D consists of five overlapping sections including collection of the undisturbed sediment-water interface, which was extruded in the field at 0.5 cm increments to 56-cm depth (Glew et al., 2001). Following whole core magnetic susceptibility measurements of the Livingston sections at 1 cm increments with a Bartington<sup>TM</sup> susceptibility meter, they were split, photographed, and visually logged for biogenic features, sedimentary structures, composition, and Munsell color. Contiguous samples were obtained at 0.5 cm or 1.0 cm increments for dry bulk density and carbon analyses. Overlapping core D sections were correlated based on visual and physical properties to produce a composite core of 250-cm length.

Core D carbonate isotope analyses was conducted on continuous 1-cm samples ( $n = 249$ ). The macroscopic carbonate particles include Charophyte stem encrustations, ostracode tests, gastropods and mollusks shells and fragments. Microscopic carbonate grains were identified as calcite and dolomite using Scanning Electron Microscopy (SEM) and Energy Dispersive Spectroscopy (EDS). Separation of fine-grained bioinduced carbonates from larger biological

and allocthonous particles, samples were wet sieved through nested screens (250, 125, 63, 32  $\mu\text{m}$ ), collected separately and freeze-dried. The finest fractions, either the  $<32\ \mu\text{m}$  size, or combined with the 32 to 64  $\mu\text{m}$  sizes if the  $<32\ \mu\text{m}$  sample was of insufficient mass, were visually examined for purity and powdered before subsampling for  $\text{CO}_2$  extraction by a Kiel automated device coupled with a Finnigan Delta 252 isotope ratio mass spectrometer. Calcite oxygen and carbon isotope ratios are reported in per mil as the relative isotope-ratio difference from VPDB defined by  $\delta^{18}\text{O}_{\text{CaCO}_3} = [({}^{18}\text{O}/{}^{16}\text{O})_{\text{CaCO}_3} / ({}^{18}\text{O}/{}^{16}\text{O})_{\text{SMOW}}] - 1$  and  $\delta^{13}\text{C}_{\text{CaCO}_3} = [({}^{13}\text{C}/{}^{12}\text{C})_{\text{CaCO}_3} / ({}^{13}\text{C}/{}^{12}\text{C})_{\text{PDB}}] - 1$ . Analytical uncertainties are  $\pm 0.05$  and  $0.1\text{‰}$  for oxygen and carbon respectively and analyses of random replicate samples fell within the range of analytical error.

Core D mineralogy was determined for samples at 2-cm increment ( $n = 151$ ) by semi-quantitative X-ray diffraction (XRD) techniques (Moore and Reynolds Jr., 1989). Each sample was packed into an aluminum holder and scanned from  $15^\circ$  to  $50^\circ$  2-theta at  $2^\circ$  2-theta/min using Ni-filtered, Cu-K $\alpha$  radiation at 45 kV, 30 ma with peak intensities recorded as counts per second (cps). Mineral identification used automated peak-search, and peak areas were quantified against standards. Results are reported as the peak intensity of the main XRD peak for each mineral and as a percentage of the sum of the main XRD peak intensities of all minerals. To improve raw XRD mineral percentage precision for the carbonate minerals of foremost interest here, the XRD data were normalized to coulometric TIC following equations in Shapley et al. (2009).

Near surface lake water samples obtained for chemistry and isotope analyses were taken in 100 ml and 30 ml HDLP Nalgene<sup>TM</sup> bottles. Isotope samples were sealed with no head space and chemistry bottle were unfiltered and acidified. Lake-water anion, cation, and alkalinity analyses were conducted at the USGS Colorado Water Science Center using standard methods

for inductively coupled mass spectrometry and chromatography. For isotope ratio analyses of water, samples were prepared by automated constant temperature equilibration by chromium reduction coupled to an isotope ratio mass spectrometer. Water isotope results are reported in per mil (‰) as the relative difference of isotope ratios ( $\delta$ ) from the international measurement standard Vienna Standard Mean Ocean Water (VSMOW) defined by  $\delta^{18}\text{O}_{\text{H}_2\text{O}} = [({}^{18}\text{O}/{}^{16}\text{O})_{\text{H}_2\text{O}} / ({}^{18}\text{O}/{}^{16}\text{O})_{\text{VSMOW}}] - 1$  and  $\delta^2\text{H}_{\text{H}_2\text{O}} = [({}^2\text{H}/{}^1\text{H})_{\text{H}_2\text{O}} / ({}^2\text{H}/{}^1\text{H})_{\text{VSMOW}}] - 1$ . Analytical uncertainties are within  $\pm 0.5\text{‰}$  and  $\pm 0.05\text{‰}$  for hydrogen and oxygen, respectively. Analyses of random replicate samples fell within the range of analytical error. Emerald Lake surface and water column measurements were collected in August 2006, with a calibrated Eureka Amphibian<sup>TM</sup> and Manta<sup>TM</sup> sonde.

The core D chronology is based on 19 AMS radiocarbon measurements of identified macrofossils. Terrestrial macrofossils were not present in sufficient quantities at some stratigraphic levels and in some cases aquatic macrofossils were used. To evaluate lake water  $^{14}\text{C}$ -reservoir effects, age offsets were determined for two pairs of terrestrial and aquatic samples obtained from the same sediment depths of 152 and 170-cm depth. Aquatic age differences of +480 and +550  $^{14}\text{C}$ -years respectively provide an average age correction of 515  $^{14}\text{C}$ -years, which was subtracted from the  $^{14}\text{C}$  ages of all aquatic samples prior to age calibration. Both measured and calibrated ages (Calib 8.2, IntCal20, Stuiver et al., 2021) are reported and calibrated ages (Cal yr BP) are used for discussion. The core A/C chronology by Morris et al. (2015) is based on 8 AMS radiocarbon ages from terrestrial macrofossils and calibrated ages are updated here using Calib 8.2 and the IntCal20 dataset.

## **Results**

## Limnology

Water column measurements for the maximum water depth of 8-m were taken in August 2006 and a thermocline was present between 5-6 m depth with the onset of a steep decline in temperatures from surface values of 16.5 to a low of 9°C. Corresponding declines with depth occurred in pH, from 8.94 to 7.13, dissolved oxygen (DO), from 9.93 to 2.93 mg/L, while specific conductivity (Spc), increased from 97 to 142  $\mu\text{S}/\text{cm}$  (Fig. 4a). The alkaline waters that are rich in dissolved calcium (Ca) are saturated with respect to calcite. Calcium exceeded magnesium (Mg) by a factor of 3 and aragonite was not observed (Table 2). Dissolved strontium (Sr) was relatively high. No evaporites were observed. Rather, exposed shorelines examined in 2009 were dominantly silt and sand sized sedimentary grains.

Table 2: Aqueous and isotopic geochemistry of Emerald Lake, Utah

Parameter	Result	
<u>Surface Water Field Measurements</u>		
Temperature (°C)	16.2	
pH	8.9	
Specific conductivity (µS/cm)	97	
Dissolved Oxygen (mg/L)	9.9	
<u>Dissolved Ions (mg/L)</u>		
Ca	21.1	
Mg	7.3	
Na	0.6	
K	0.27	
Alkalinity	75.2	
Cl	0.62	
SO <sub>4</sub>	2.3	
Sr	107	
<u>Carbon and Oxygen Isotopes (‰VPDB)</u>	<u>δ<sup>18</sup>O</u>	<u>δ<sup>13</sup>C</u>
Lake water (2006)	-12.1	na
Lake water (2007)	-11.1	na
Surface sediment	-11.50	1.87
Predicted equilibrium value <sup>1</sup>	-11.23	
Living Chara	-13.09	-2.56
Bedrock (Flagstaff Fm)	-5.70	-8.31

<sup>1</sup>Following the equations of Epstein et al. (1953), Tarutani et al. (1969), Friedman and O’Niel (1977)

### *Isotope Hydrology*

The water isotope values of Emerald Lake water were -12.1 and -11.1‰ and -98 and -94‰ for  $\delta^{18}\text{O}$ ,  $\delta^2\text{H}$ , 2006 and 2007, respectively and plot on a local evaporation line (LEL) defined by the regression of values from local high plateau lakes and springs with a slope of 4.9 ( $R^2 = 0.98$ ; Supplemental Information). Seasonal precipitation isotopes values for Utah from Friedman et al. (2002b) define a local meteoric water line (LMWL) with a slope of 7.7 and  $\delta^{18}\text{O}$  range between -2 and -20‰ (1991 -1996, Brian Head, Cedar City, Delta, Hanksville and Price, also see (Marchetti et al., 2018). The intersection of the LEL with the LMWL, and the global meteoric water line (GMWL, slope = 8) provides an estimate for the  $\delta^{18}\text{O}$  of mean annual precipitation between -15 and 16 ‰ similar to other regional with a snow-dominated seasonal precipitation balance (Anderson et al., 2016a). Lake water isotope values along the LEL trajectory away from the intercept reflects progressive enrichment in heavy isotopes ( $^{18}\text{O}$  and  $^2\text{H}$ ) in response to evaporation. The position of Emerald Lake on the LEL indicates evaporative enrichment of  $\sim +4\text{‰}$  for  $\delta^{18}\text{O}$ , reflecting moderate sensitivity compared to values upwards of  $\sim 8\text{‰}$  at other lakes in similar settings. Interannual variations in the  $\delta^{18}\text{O}$  values of mean annual precipitation typically within a smaller range of 2‰ (Friedman, 2002b).



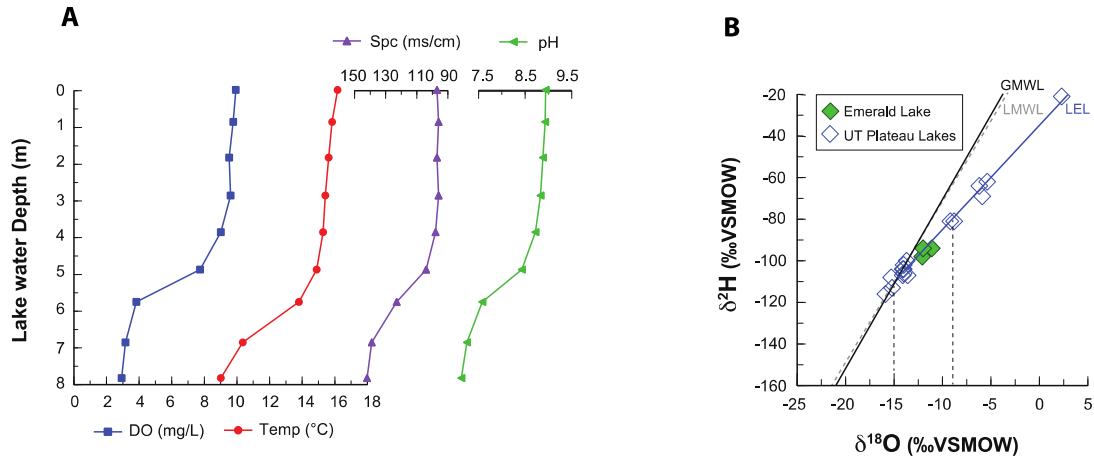


Figure 4: Emerald Lake water column measurements (A) and lake water isotope ratios shown with nearby High Plateaus lakes that form a local evaporation line (LEL) with a lower slope than the global and local meteoric water lines (GMWL, LMWL, LMWL from Friedman et al. 2002).

### Core lithologies

Core D was divided into four limnic facies based on color, structure, texture, and bulk sedimentary compositions (Fig. 5). From the base of the core moving upwards, Unit I (250-240 cm depth, ~7150 to 6750 cal yr BP) is composed of faintly bedded light gray clayey silt. Aquatic macrofossils include trace shells (likely *Psidium*), *Chara* oogonia and fine fragments of root vegetation. *Picea* needles, cone and bark fragments occur near the upper boundary (Supplemental Information). The relatively high basal values in magnetic susceptibility (~1.5 SI) and dry bulk density ( $0.75 \text{ g/cm}^3$ ) steadily decline upwards as percentages of organic matter (%OM) rise (<5% to 20%) and inorganic carbonate decline (70 to 40%).

The transition to Unit II (239 to 170 cm, ~6750 to 5530 cal yr BP) is marked by a color shift to light gray olive brown mottled marl with occasional dark olive gray bands. The marl is abundant in herbaceous aquatic material, and contains *Potamogeton* seeds, gastropods, daphnia remains and fine roots. Terrestrial macrofossils include insect parts, charcoal, bark and cone fragments, and needles of *Picea* and *Pseudotsuga*. Low magnetic susceptibility (<1SI) and dry

bulk density ( $\sim 0.2 \text{ g/cm}^3$ ) reflect the higher %OM (20 to 40%) and carbonate (40 to 75%).

Although mottled, the marl is strongly bedded, with alternating bands of slightly lighter and darker olive brown color.

The transition to Unit III is an unconformable change in texture and composition to solid monochromatic silty gyttja (171 to 110 cm depth, 5530 to 2250 cal yr BP) interpreted as a non-conformable surface. The horizon is marked by an abrupt rise in magnetic susceptibility and %OM as carbonate declined from  $\sim 70$  to 20%. Above the unconformity, dry bulk density values and color banding remain unchanged while the bedding becomes diffuse. At 152 cm depth, a very large wood bark fragment occurs with peak values of magnetic susceptibility when carbonate is entirely absent. Above this depth a gradual rise in carbonate is tracked by declines in magnetic susceptibility and %OM. Macrofossils in Unit III are significantly less abundant than all other units and where present are dominated by undifferentiated aquatic herbaceous material.

The transition to the base of Unit IV (110 to 0 cm depth, 2250 cal yr BP to present) is a gradual return to mottled textures and higher percentages of carbonate ( $>40\%$ ) with a decline in magnetic susceptibility values. Unit IV has similar macrofossil types as Unit II, rich in *Picea* needles and includes *Chara* stem casts while lacking oogonia and daphnia. A complete and intact conifer cone occurs at 97 cm depth.

### **Emerald Lake, Utah core D07**

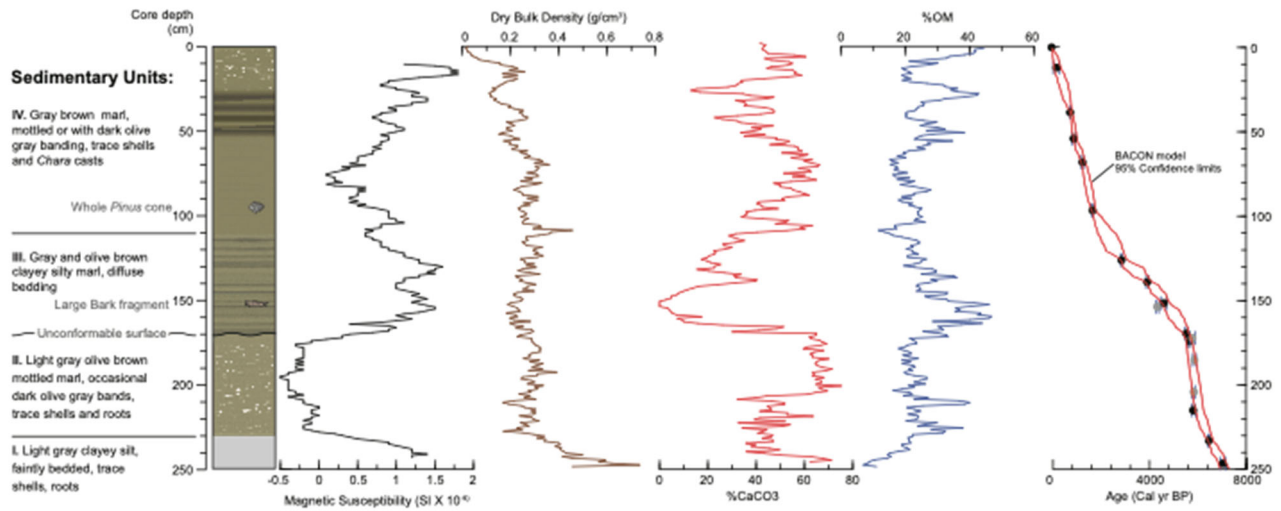


Figure 5: Core D lithologic units, bulk magnetic susceptibility (black) and dry bulk density (brown), percent inorganic carbon (red) and organic matter (blue), and the age-depth model. Age control points are shown in black with 1-sigma error bars. Omitted ages are shown in gray. Red outlines denote the 95% confidence limits of the age model.

Core A/C is divided into two limnic facies (Supplemental Information). Basal Unit I (296 to 244 cm) is bedded silty olive brown marl, with intermittent mottling, and high yet variable values of dry bulk density (0.4 to 0.6 g/cm<sup>3</sup>), percent carbonate (2- to 40%), and %OM (20-40%). Near the upper boundary of Unit I are occasional mm-scale white bands before transition to massive olive brown gyttja, which characterizes Unit II (244 to 0 cm). Moving upwards through Unit II, dry bulk density values gradually decline to values near 0.1 g/cm<sup>3</sup> for the upper 50-cm of the core. Throughout Unit II %OM fluctuates between 25 and 40%, whereas percent carbonate is near zero at the base and gradually rises and remains near ~25% before a decline to near zero in the upper 30 cm.

### *Age Models and Sedimentation Rates*

Age-depth models were generated using the Bayesian software ‘rbacon’ package v.2.5.3 in R (Blaauw et al., 2021; Blaauw and Christen, 2011), which includes IntCal20 calibrations.

Default prior assumptions were used. For core D, three aquatic samples at 173, 186, and 295 cm depth were omitted because the median calibrated ages were statistically identical to one another within the range of 1-sigma error. The resulting model for Core D has an average error range of  $\pm 170$  years with a maximum of  $\pm 330$  years between 100 and 150 cm depth, where a single potamogeton seed at 139 cm was the only suitable material to be found. The average rate of core D sediment accumulation is  $0.06 \pm 0.07$  cm/yr. Maximum rates of 0.26 cm/yr occur within Unit II, between  $\sim 6000$  and 5600 cal yr BP, below the unconformity. Minimum rates of 0.012 cm/yr occur within Unit III between 4000 and 2800 cal yr BP.

For core A/C, an unusually old age at 81 cm depth of 2520 cal yr BP was omitted because it generated unrealistic changes in sedimentation rates. The resulting error range for core A/C age is larger than core D, with an average of  $\pm 300$  years and maximum of  $\pm 700$  years where ages were extrapolated to the bottom of the core (Supplemental Information). Core A/C sediment accumulation rates are  $0.06 \pm 0.06$  cm/yr with maximum rates of 0.25 cm/yr occur within the upper 5 cm which represents that past  $\sim 50$  years. Minimum rates of 0.010 cm/yr occur at the base of the core from  $\sim 10,000$  to 6500 cal yr BP.

Table 1 Emerald Lake, Utah, radiocarbon data

Core Depth (cm)	Material	$^{14}\text{C}$ Age ( $^{14}\text{C}$ yr BP)	Measured Reservoir Offset	Reservoir Corrected $^{14}\text{C}$ Age ( $^{14}\text{C}$ years)	AMS $^{14}\text{C}$ Lab # <sup>c</sup>	$\delta^{13}\text{C}$ (‰ VPDB)	M Ca
D07							
0	Core top	n/a					
12	Wood and Picea needle	$150 \pm 20$			CURL-17633	-26	
39	Conifer bark	$815 \pm 15$			CURL-12003	-25.6	
54	Conifer needles	$970 \pm 25$			CURL-16693	-25	
68	Wood	$1295 \pm 15$			CURL-12007	-26.2	
97	Conifer cone whole	$1745 \pm 20$			CURL-12011	-22.7	
126	Potamogeton Seed	$3279 \pm 35$		$2755 \pm 35$	USGS-1526		
139	Picea wing fragments	$3600 \pm 25$			CURL-17640	-23.3	
152	Conifer bark	$4095 \pm 20$			CURL-12005	-23.4	
152	Comparison aquatic	$5320 \pm 30$	480		USGS-1499		

154	Conifer bark	3865 ± 30		WW-9129	-22.1
170	Picea needle, leaf scar, wood, charcoal	4770 ± 40		USGS-1500	
170	Comparison aquatic	5320 ± 30	550	USGS-1501	
173	Aquatic	5530 ± 20	5015 ± 20	USGS-1502	
174	Aquatic	5450 ± 30	4935 ± 30	WW-9130	-16
186	Aquatic	5570 ± 20	5055 ± 20	USGS-1620	
205	Aquatic	5735 ± 25	5107 ± 25	USGS-1621	
215	Wood	5110 ± 20		USGS-1622	
233	Conifer needle	5685 ± 20		CURL-13023	-21
247	Conifer cone fragments	6140 ± 30		USGS-1338	-25
A/C07 <sup>b</sup>					
0	Core top				
24	<sup>210</sup> Pb horizon				
38	Charcoal	735 ± 15		CURL-18264	
67	Charcoal	1280 ± 15		CURL-18248	
81	Conifer needle	2451 ± 27 <sup>a</sup>		CAIS-4785	
120	Conifer needle	1617 ± 26		CAIS-4787	
154	Conifer needle	2985 ± 24		CAIS-4789	
199	Conifer needle	3843 ± 27		CAIS-4791	
244	Conifer needle	5381 ± 28		CAIS-4793	
284	Conifer needle	8483 ± 26		CAIS-4795	

<sup>a</sup>Not used in age model

<sup>b</sup> By Morris et al. (2015) and calibrated with v.8.2.1(IntCal20) from <sup>14</sup>C ages in

<sup>c</sup> CURL = Institute of Arctic and Antarctic Research (INSTAAR) Radiocarbon Laboratory, USGS = USGS Geoscience and Environment Change Science Center Radiocarbon Laboratory, WW = USGS Reston Radiocarbon Laboratory, CAIS = Univ. of Georgia Center for Applied Isotope Studies

## Mineralogy

Core D mineral compositions are composed of calcite with lesser dolomite, quartz, and feldspar, which are detrital minerals in this setting (Fig. 6). Prominent mineralogic change correspond with the four lithic units that are hereafter described by age. Between 7150 and 5530 cal yr BP, in Units I and II, calcite is dominant (40-60%) with minor quartz (~10%), trace dolomite and feldspar (<3%). At ~5500 cal yr BP, an abrupt rise in dolomite (+25%) and quartz

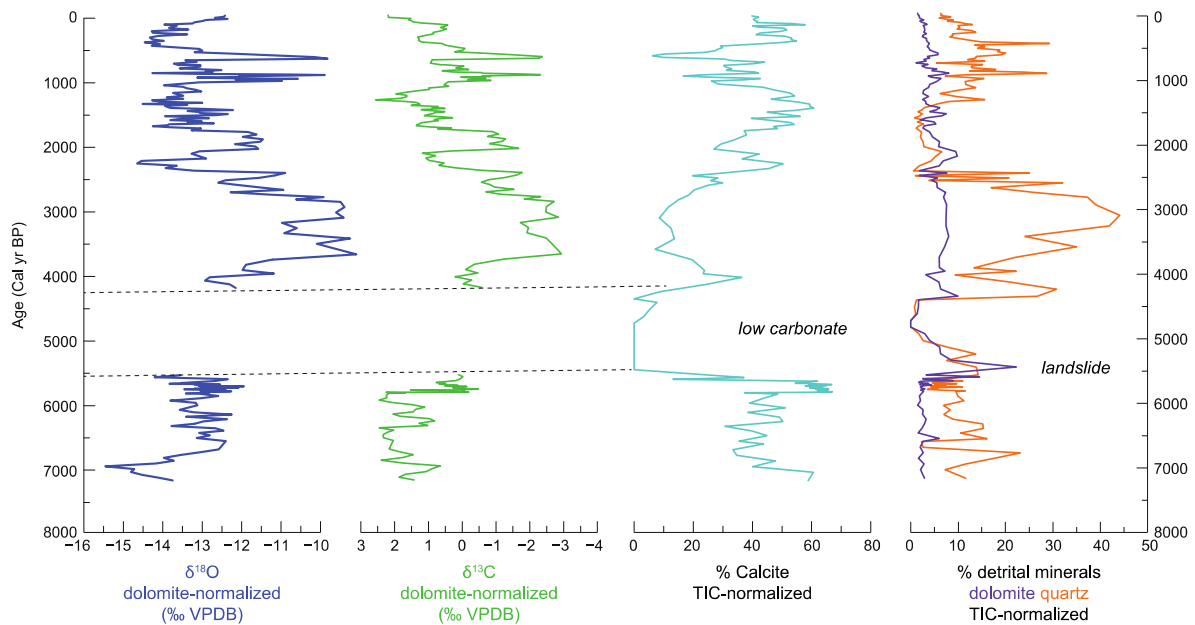


Figure 6: Core D07 carbonate  $\delta^{18}\text{O}$  and  $\delta^{13}\text{C}$  (dolomite-normalized, note reversed axis) shown with abundances of calcite, dolomite, and quartz (as percent of whole sediment). Percentages of dolomite are an indicator of detrital influence on calcite abundance and is used to normalize the isotope values of carbonate isotope values. Mineral abundances are normalized by percent carbonate using coulometric values of Total Inorganic Carbon (TIC).

(+5%) occur with major decline in calcite (-60%) that coincides with the depth of the unconformity at the base of Unit III. During the next several centuries calcite was absent as dolomite and quartz gradually declined to trace values by ~5000 cal yr BP. By ~4700 cal yr BP trace amounts of calcite reappeared intermittently before an abrupt rise in quartz (+30%) at ~4500 cal yr BP, which became the dominant mineral (up to 45%) between ~4500 and 2650 cal yr BP, with minor calcite (10 to 20%) and trace dolomite (~5%). Over the next several centuries (~2650 and 2450 cal yr BP) quartz values declined precipitously to trace levels, with several rapid fluctuations of 20 to 30%, as calcite increased by +40% to become the dominant mineral (>50%) in Unit I. Within Unit I, briefly lower calcite abundances occurred during short peaks in quartz (~30%) at ~890 and 425 cal yr BP.

### *Carbonate Stable Isotopes*

Isotope results of bulk carbonate reflect varying proportions of endogenic calcite and detrital dolomite and detrital calcite. A binary endogenic calcite and detrital dolomite mixture is assessed by taking the fraction of dolomite (of total carbonate) multiplied by Flagstaff dolomite values of -5.7‰ for  $\delta^{18}\text{O}$  and -8.3‰ for  $\delta^{13}\text{C}$  (Bowen et al., 2008), subtracted from raw  $\delta^{18}\text{O}$  and  $\delta^{13}\text{C}$  values, respectively, and divided by the fraction of calcite of total carbonate.

$$\delta^{18}\text{O}_{\text{Norm}} = (\delta^{18}\text{O}_{\text{raw}} - f_{\text{dolomite}} \times -5.7) / f_{\text{calcite}}$$

and

$$\delta^{13}\text{C}_{\text{Norm}} = (\delta^{13}\text{C}_{\text{raw}} - f_{\text{dolomite}} \times -8.3) / f_{\text{calcite}}$$

The result of the dolomite normalization is to lower raw carbonate isotope values by as much as -2‰ for oxygen and carbon, in proportion to abundance (Supplemental Information). Normalized  $\delta^{18}\text{O}$  values range from ~-9 to -16‰ and  $\delta^{13}\text{C}$  values from ~2 to -2‰ while the structure of the raw stratigraphic isotopic trends remains intact. The variations in the proportion of detrital calcite may vary equivalently with dolomite, but this is uncertain. For example, there are differences in variations between dolomite and quartz. If detrital calcite were equivalent in proportion to dolomite, then normalization results in an additional lowering by ~ -2‰ for oxygen and carbon (Bowen et al., 2008), in proportion to abundance, and again without altering raw stratigraphic trends. The dolomite-only normalization is an intermediate solution and stratigraphic variations are treated appropriately for interpretation within the known range of uncertainty.

Dolomite-normalized values of  $\delta^{18}\text{O}$  between ~7150 and 6750 cal yr BP (Unit I) vary between -14 and -16‰ (Figure 6). From 6750 to 5530 cal yr BP (Unit II) values increase,

varying between -13.5 and -12.5‰. The loss of carbonate at the time of unconformity, ~5500 cal yr BP, interrupts the isotope record and no data could be obtained (Unit III). The  $\delta^{18}\text{O}$  record resumes at ~4000 cal yr BP (Unit IV) with an increase in values to -10‰ at ~3500 cal yr BP, which coincides with high proportions of detrital quartz. At ~2500 cal yr BP values precipitously declined to -14.5‰ in less than 500 years, with a corresponding decline in detrital quartz. Subsequently, when detrital minerals were at trace levels,  $\delta^{18}\text{O}$  values abruptly rose to ~-12‰ by ~2000 cal yr BP and declined to ~-14.5‰ by ~1600 cal yr BP. For the past ~1500 years, values varied between -14 and -13‰. The exceptions were two prominent positive excursions to values near -10‰, which coincided with a rise in detrital quartz at ~890 and 425 cal yr BP.

Dolomite-normalized values of  $\delta^{13}\text{C}$  covary with  $\delta^{18}\text{O}$  values that are greater than -12‰ in a manner that is observed for hydrologically closed lakes (Horton et al., 2016; Talbot, 1990), and which also coincide with higher proportions of detrital minerals (Fig. 7). Low  $\delta$ -values in both isotopes are more widely scattered, which is more frequently observed for lakes with shorter residence times and higher hydrologic connectivity through sub-surface flow. Higher carbonate abundance in Emerald Lake is related to lower lake- $\delta^{18}\text{O}$  values, a relationship that has previously been observed to indicate that reductions in calcium-rich groundwater inflow in response to dry conditions can also impose limitations on carbonate production (Shapley, 2005).



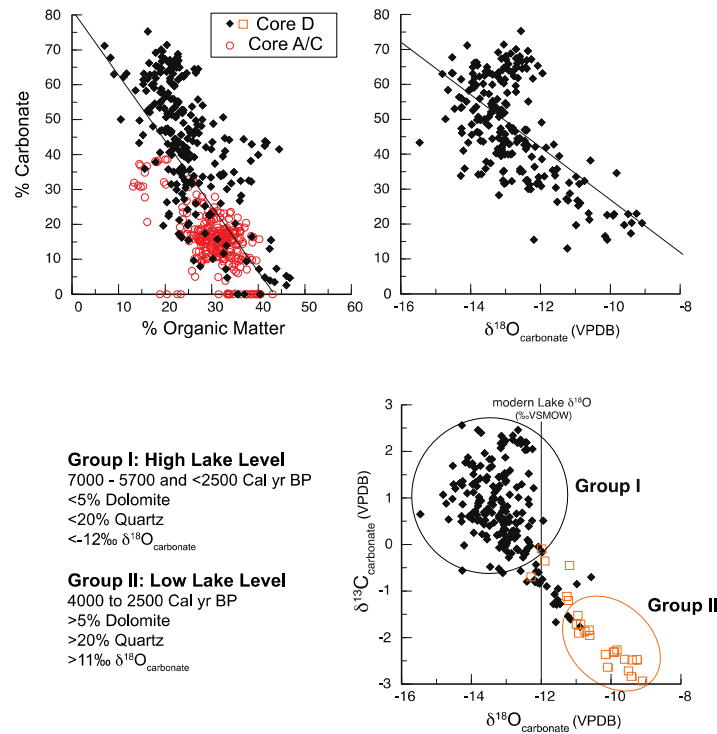


Figure 7: Sediment associations for (a) organic matter and carbonate abundances (core D in solid black, core A in open red), (b) percent carbonate and carbonate  $\delta^{18}\text{O}$  (dolomite normalized), and (c) carbonate  $\delta^{18}\text{O}$  and  $\delta^{13}\text{C}$  (dolomite normalized) grouped by detrital mineral abundance (higher in open orange) and inferred lake level.

## Discussion

The results from Emerald Lake are discussed first in terms of lake-level change, including the landslide event, based on the interpretation of sedimentology, mineralogy, and geochronology from both sediment cores A/C and D (Figs. 8 and 9). This is followed by a rationale for the carbonate oxygen isotope interpretation of core D and the paleoclimatic reconstruction for the high plateau region of central Utah (Figure 10). This is followed by comparison with regional records in the Upper Colorado river basin, the Great Basin, and the Northern Rocky Mountain regions, including comments regarding the ‘Late Holocene Dry Period’ (Mensing et al., 2013).

### *Holocene lake levels and landslide activity*

After Pleistocene glaciers receded on the Wasatch Plateau, early Holocene limnic sedimentation in the Emerald Lake basin by ~10,000 cal yr BP is based on an age from core A/C that is ~40 cm above the base. The onset could be as early as ~11,300 cal yr BP if age model extrapolation to the base of the core is accurate (Fig. 8). Relatively dry early Holocene conditions are indicated by slow sedimentation rates, while high carbonate preservation suggests that the early lake was too shallow to support extensive carbonate dissolution within the water column (< 4-m depth; Fig. 4a). Significant organic matter accumulation indicate that the early shallow pond was biologically productive. This is consistent with pollen indicators for cattail (*Typha* spp.) and willow (*Salix* spp.) within a sub-alpine spruce-fir forest. Relatively low charcoal levels indicate infrequent and relatively mild severity fire (Morris et al., 2015).

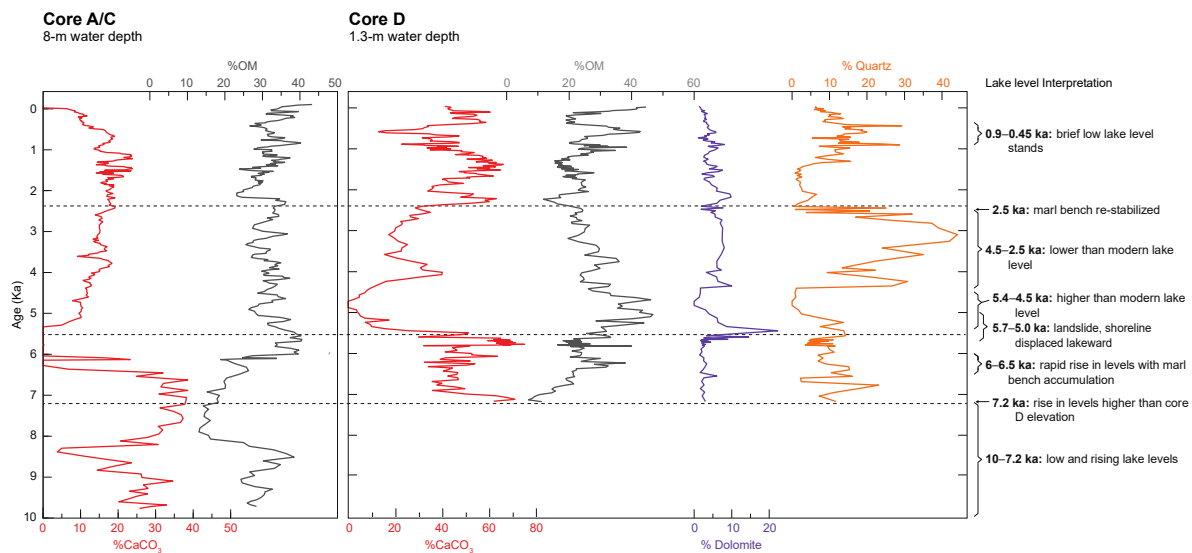
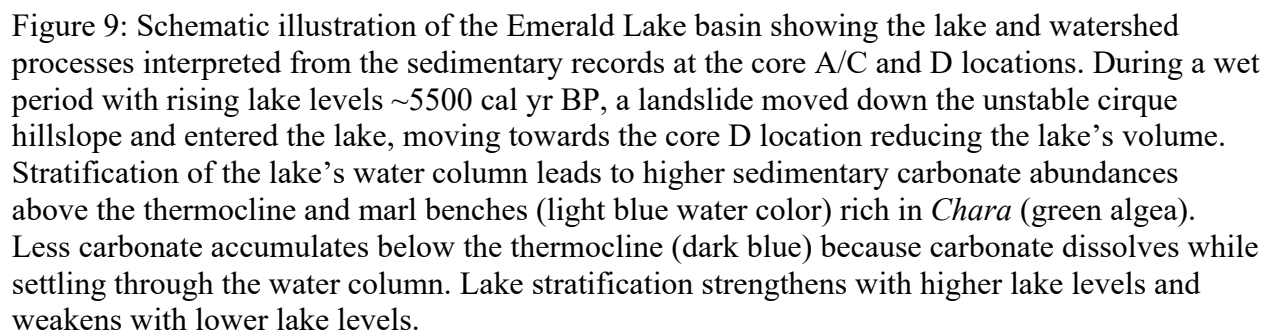


Figure 8: Stratigraphic variations in sediment composition for core A/C (left, 8-m water depth) and core D (middle, 1.3-m water depth) with chronological lake level interpretations (right). All units are in percent for carbonate (red, %CaCO<sub>3</sub>), organic matter (black, %OM), and for core D, detrital dolomite (purple) and quartz (orange).

After ~8500 cal yr BP, higher carbonate in core A/C, and corresponding decline in organic matter, vary in manner in which organic carbon production is negatively associated with carbonate preservation and commonly known as the ‘carbon pump’ (Dean, 1999; Fig. 7). Rising carbonate amounts could also indicate reworked material from early development of the marl bench around the margins of the lake’s depocenter (Fig. 9 and Fig 3b).

By ~7,200 cal yr BP marl accumulation began at the core D location while carbonate abundance in deeper water depths remained unaltered, indicating that lake levels had risen to maximum water depths of ~5 to 5.5 m, accounting for sediment depths at core D of <0.1-m at that time. Subsequently rapid shallow water marl accumulation (~50-cm) between ~6500 and 5500 cal yr BP indicates rising lake levels to depths of > 6.5 to 7 m. The corresponding carbonate decline in core A/C suggests a deeper water column, enhanced stratification, and higher carbonate dissolution. This lake levels rise during the early-to-mid Holocene indicate a rise in precipitation minus evaporation (P-E) during quiet fire conditions (Morris et al., 2015) when the landslide movement down the cirque face into Emerald Lake occurred.

The landslide is interpreted from the sediments of proximal core D by 1) a sedimentary unconformity, 2) disappearance of endogenic carbonate, and 3) a pulse in detrital minerals, all at a stratigraphic position which immediately overlies a radiocarbon age of at  $\sim 5520 \pm 50$  cal yr BP. Additionally, carbonate increased in deep water depths, which is consistent with remobilization of shallow sediments with lakeward shoreline movement. The detrital pulse suggests an initially rapid slump release followed by sediment delivery by surface runoff. The radiocarbon ages above and below the unconformity are continuous and abrupt reduction in sedimentation indicate that the front likely slowed as it moved towards the core D location with minor or no erosion,



After the post-landslide period, a prominent rise in quartz at the core D location began at ~4500 cal yr BP that is distinct from the inferred landslide detrital signature. Although the initial increase in quartz was similar, with a pulse in dolomite, the dolomite rise was smaller and then declined to trace levels as quartz continued to rise and remain elevated for the subsequent ~2000 years. In further contrast to the post-landslide period when endogenic carbonate disappeared, endogenic carbonate began to gradually increase. The interpretation is that quartz reflects the winnowing of nearshore sediments in response to lake level declines of 1 to 2 m below previous levels, accounting for ~1 to 1.5- m sediment thickness of core D at that time. The inferred lake level decline during this period coincides with an increase in charcoal abundance reflecting increased fire frequency and severity (Morris et al., 2015). The lake's deep water sediments were unaffected by the lake level decline because it did not alter lake stratification or rates of carbonate dissolution. The increase in shallow water detrital quartz corresponds with inhibited marl bench growth indicated by reduced sedimentation rates. *Chara* thrives in undisturbed clear water in calm offshore areas, conditions that appear to return by ~2500 cal yr BP with quartz declines and rising water levels to modern conditions. During the past ~2500 years, near modern lake levels indicate relatively wet conditions compared to mid and early Holocene periods, although brief low stands and dry periods are indicated by higher frequency variations in quartz.

#### *Oxygen isotope interpretation and paleoclimatic reconstruction*

The stratigraphic variations in sedimentary carbonate  $\delta^{18}\text{O}$  values (dolomite-normalized) are interpreted as a proxy for variations in lake- $\delta^{18}\text{O}$  values based on the modern data (Table 2), which indicate that carbonate sediments of endogenic origin are in isotopic equilibrium with lake water. In turn, Emerald lake- $\delta^{18}\text{O}$  is influenced by P-E and shifts in the relative proportions of

winter and summer precipitation, which strongly covary with precipitation source and temperature (Fig. 4b). Higher lake- $\delta^{18}\text{O}$  values indicate increased rates of evaporation during the ice-free season from June through September, relative to precipitation, resulting in lower P-E. Higher values may also reflect more summer rainfall relative to winter snowfall. Summer rainfall in central Utah is associated with warmer temperatures and convection of recycled moisture derived from the south (Anderson, 2012; Friedman, 2002a). In contrast, lower lake- $\delta^{18}\text{O}$  values indicate higher rates of precipitation resulting in higher P-E. Lower lake- $\delta^{18}\text{O}$  values may also reflect more winter snowfall relative to rainfall. In central Utah, winter snowfall is associated with cold temperatures and North Pacific moisture sources.

The resulting Emerald lake- $\delta^{18}\text{O}$  inferred paleoclimatic interpretation is described in terms of anomaly values relative to the Holocene average of -12.8‰ (Figure 10), which is similar to the values of the modern lake. This approach is warranted by the influence that changes in the proportions of detrital carbonate can exert on absolute  $\delta^{18}\text{O}$  values and differences. For example, the detrital influence on the sensitivity of the  $\delta^{18}\text{O}$  proxy is most pronounced during low lake stands. The interpretation of the lake's volumetric and isotopic evolution in response to P-E is carefully framed by the lake level reconstruction.

Negative lake- $\delta^{18}\text{O}$  anomalies from ~7200 to 6800 cal yr BP are attributed to higher P-E when lake levels were rising, and the lake's surface area expanded over the core D location. The early negative lake- $\delta^{18}\text{O}$  anomalies could reflect spring discharge points, which have relatively low  $\delta^{18}\text{O}$  values and may have been active at the shoreline when it was near the core D location. They could also be interpreted to reflect higher snowfall proportions, yet in the context of regional comparisons this is a less likely explanation as discussed in further detail below. Lake- $\delta^{18}\text{O}$  anomalies were positive by ~6600 cal yr BP and are interpreted to reflect a rain-dominated

precipitation balance when lake levels rose in response to higher P-E. Lake- $\delta^{18}\text{O}$  anomalies subsequently fluctuated near the Holocene average in apparent isotopic steady state as lake levels rose with marl bench sedimentation. That the landslide at ~5500 cal yr BP occurred during relatively wet paleohydrologic conditions implicates a climatic trigger for the slope failure (e.g., Shurtliff et al., 2017). However, there is currently no evidence that allows rejection of a seismic trigger related to any of the numerous faults within the area (Machette et al., 1991).

Between ~4000 and 2500 cal yr BP, positive  $\delta^{18}\text{O}$  anomalies reflect low lake levels driven by low P-E. The interval is exceptional in duration and by showing levels of aridity that approach those of the early Holocene. By ~2800 cal yr BP, a return to wet conditions driven by higher amounts of snowfall relative to rainfall was underway, reflected by a shift to negative lake- $\delta^{18}\text{O}$  anomalies between ~2200 and 2000 cal yr BP. A rapid shift from negative to positive anomalies between ~2000 and 1800 cal yr BP indicate low P-E, which was relatively brief by comparison with previous dry periods. Subsequently, a wetter, cooler, snow-dominated climatology persisted between ~1800 and 1000 cal yr BP with negative lake- $\delta^{18}\text{O}$  anomalies in an apparent isotopic steady state. Hydroclimatic variations became more frequent during the Medieval Climate Anomaly (MCA; AD 1250 to 950) with rapid shifts to low lake levels and P-E between ~1000 and 700 cal yr BP, caused by reductions in winter precipitation that may have included failed summer rains. In contrast, a wet, cool, snow-dominated climatology dominated the Little Ice Age (LIA; AD 1300 to 1850) to cause persistently negative lake- $\delta^{18}\text{O}$  anomalies. By comparison, reduced snowfall and P-E characterize the past ~100 years that approximate the Holocene, average.

### *Regional Comparison*

The high elevation paleoclimatic reconstruction in central Utah from Emerald Lake based on carbonate oxygen isotope data show paleoclimatic variations at time scales ranging from millennia to decades and geographical comparison between the Great Basin of eastern Nevada and the Upper Colorado River basin (Figure 10). Relatively low P-E that was gradually rising between ~10,000 to 7000 cal yr BP, indicated by low and rising Emerald Lake levels compared to present, correspond with orbital forcing by trends in summer solar insolation that are consistent with strengthened monsoon rainfall (relative to snow) with northward retreat of the Laurentide Ice sheet (Anderson, 2011; Bhattacharya et al., 2018; Epstein and Xu, 1999; Huth et al., 2020; Metcalf et al., 2015; Sjostrom et al., 2004). Higher early Holocene soil infiltration trends at locally low elevations are inferred from isotopes of laminated soil carbonate rinds in Torrey, Utah (~1080 m elevation; (Huth et al., 2020). An early Holocene rise local P-E at Garden Basin Fen (2400-m elevation) on the slope of the Fish Lake Plateau, inferred from pollen and diatom assemblages, corresponds with timing of the Windy Ridge landslide (Shurtliff et al., 2017). While sub-regional climatic variations are inherently intricate, the collective evidence support increased early Holocene effective moisture at latitude ~39 to 40° N, across the Upper Colorado River Basin, from central Utah at Emerald Lake to northwest Colorado which included contributions from southerly moisture sources usually associated with the monsoon.

The rise to near modern Emerald lake-levels by ~7500 cal yr BP and continued rise through at least ~5500 cal yr BP, with  $\delta^{18}\text{O}$  variations near both modern and Holocene averages, is indisputable evidence for rising P-E during the mid-Holocene by comparison to the early Holocene. Additional evidence for higher P-E during this period from eastern Nevada includes initiation of the Spring Valley (1910 m elevation) sedge-meadow by ~7500 cal yr BP, return of marshes at the Blue Lake wetland by ~6500 cal yr BP, and early lake development in the



Pahranagut Valley (975 m elevation) by ~5800 cal yr BP (Louderback and Rhode, 2009; Mensing et al., 2013; Theissen et al., 2019). To the east in Colorado, gradual decline in precipitation  $\delta^{18}\text{O}$  values at Bison Lake during this period, and overflowing lake levels at Yellow Lake (3090 m elevation), indicate a gradual increase in snowfall relative to rain (Anderson, 2012). While the landslide into Emerald Lake at ~5500 cal yr BP was a direct cause for an abrupt rise in lake level, higher levels may have subsequently stabilized between ~5500 and 4000 cal yr BP in part due to higher P-E, although this is not certain. Lake level evidence in the central Colorado Rockies indicate rising P-E between 5700 and 4800 cal yr BP (Shuman et al., 2014).

In contrast to the evidence presented here, Lachniet et al. (2020) proposed aridity intervals at Leviathan cave between ~9000 and 5000 cal yr BP based on elevated  $\delta^{18}\text{O}$ ,  $\delta^{13}\text{C}$ , and slow growth rates. The elevated cave water  $\delta^{18}\text{O}$  values are also attributed to warmer temperatures, and reasonable alternatives to their plausible explanations could also include southerly moisture sources usually associated with the monsoon (e.g., Huth et al., 2020). The Leviathan  $\delta^{18}\text{O}$  record shows a millennial scale decline between ~8000 and 5000 cal yr BP, which to some extent could reflect regional rise in P-E described here. Nevada speleothem  $\delta^{18}\text{O}$ ,  $\delta^{13}\text{C}$ , and trace element records also show contrasting trends in different caves (Lachniet et al., 2014; Steponaitis et al., 2015) and differences in cave hydrology and/or disequilibrium with elevation are known to influence speleothem proxy sensitivity in unique ways (e.g., Johnston et al., 2013; Weber et al., 2021). In addition to cave drip water studies that investigate isotopic relationships with those of meteoric water (Oster and Kelley, 2016), further investigations into isotopic relationships with surface waters are needed, since these water sources, rather than direct precipitation, are often what are incorporated into stalagmite proxies (Anderson et al., 2016b).

Following the landslide at ~5500 cal yr BP at Emerald Lake, and a relatively wet period thereafter, there began a multi-millennial dry period between ~4000 and 2400 cal yr BP which envelopes a previously identified “Late Holocene Dry Period” (Mensing et al., 2013), which further extends the spatial and temporal extent of this episode. The timing of increased Emerald lake- $\delta^{18}\text{O}$  and detrital minerals between ~4000 and 3500 cal yr BP corresponds with increased lake- $\delta^{18}\text{O}$  in Yellow Lake. Thereafter, the record comparison suggests time-transgressive drought expansion based on increased lake- $\delta^{18}\text{O}$  at Pahranaugut that occurred several centuries later, which was then followed by the rise in carbonate preservation at Stonehouse Meadow (attributed to dry conditions) which occurred another several centuries later.

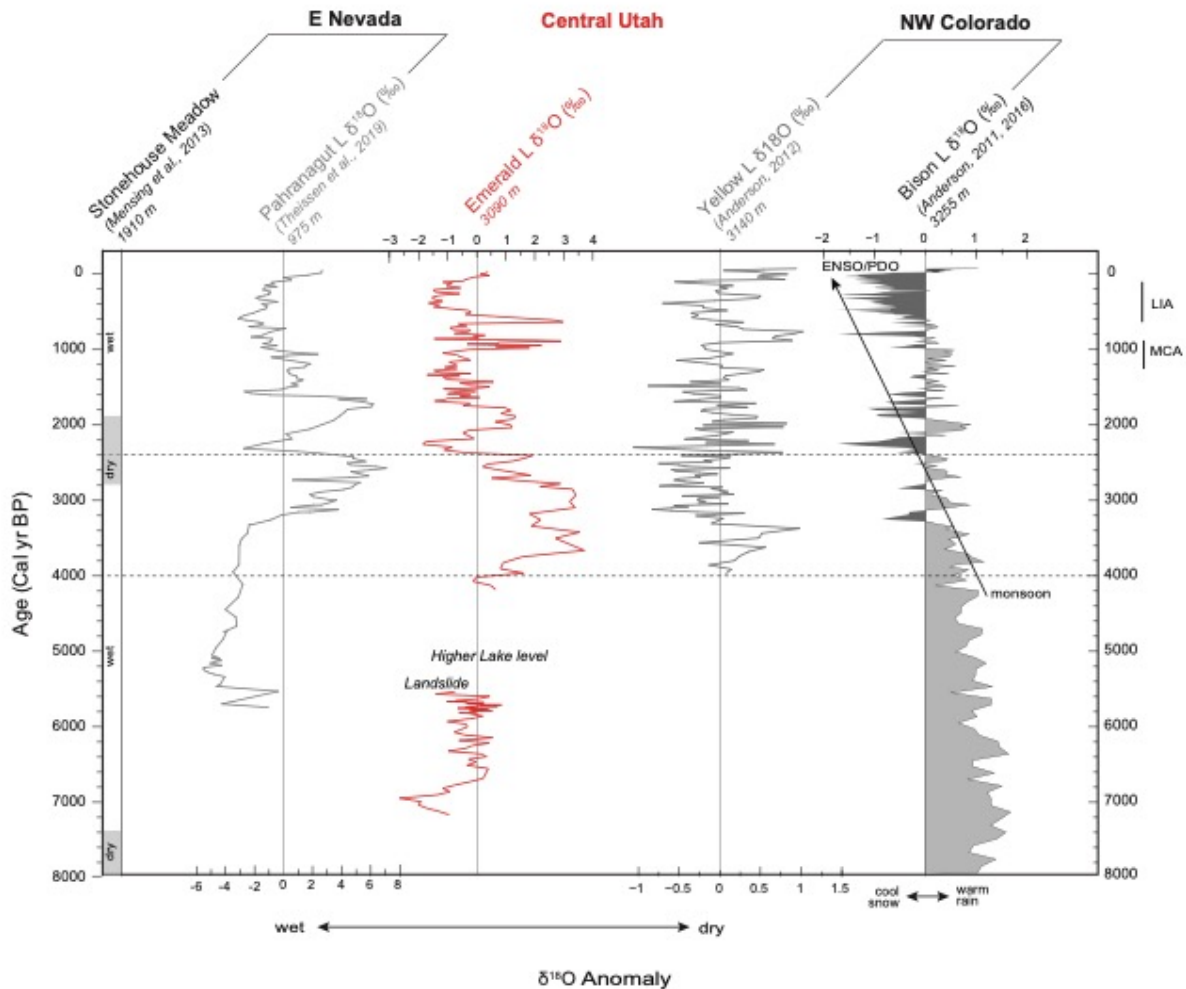


Figure 10: Regional record comparison between latitude 37° and 40°N from west (left, -114.5°W, eastern Nevada) to east (right, -107°W, western Colorado): inferred wet and dry periods at Stonehouse Meadow (1910 m elevation; Mensing et al., 2013);  $\delta^{18}\text{O}$  anomalies at Pahrnagut Lake (975 m elevation; Theissen et al., 2019), Emerald Lake (red) in central Utah (3090 m elevation, this study) and Yellow and Bison Lakes (3140 m and 3255 m elevation, respectively; Anderson, 2011 and 2012; Anderson et al., 2016a and 2016b).

The temporal differences of these shifts may approach the chronological uncertainties of the independent age models (e.g., Zimmerman and Wahl, 2020) leaving the possibility that the some or all of the shifts were either nearly simultaneous, or that the progression of the pattern was slower or faster within a few centuries. However, it is interesting to note that the timing of a notable decline in Emerald, Yellow and Pahrnagut lake- $\delta^{18}\text{O}$  at ~2,200 cal yr BP, within the dry period, precisely coincides with the earliest negative lake- $\delta^{18}\text{O}$  anomalies of the Bison Lake record, to suggest that a region-wide period of higher snow (relative to rain) interrupted the extended drought.

While the onset of the dry period was transgressive, its termination at ~2400 cal yr BP was rapid and regional with near synchronous declines in lake- $\delta^{18}\text{O}$  registered at Pahrnagut, Emerald, Yellow and Bison, indicating a shift to high snowfall (relative to rain) that increased P-E. By ca. 2000 cal yr BP, a rapid return to dry conditions was simultaneously registered by increased lake- $\delta^{18}\text{O}$  at all four of the sites, which persisted for multiple decades to centuries, and corresponds with multi-decadal drought recorded by tree-ring chronologies in northeastern Utah and southern San Juan Mountains (Knight et al., 2010; Routson et al., 2011). This early first millennium dry period is not so clearly registered in northwestern Colorado at Bison and Yellow lakes, which indicate high snowfall and P-E variations near the Holocene average. If this difference represents an east-west precipitation pattern, it is consistent with anomalously persistent atmospheric ridging over the Great Basin and jet stream flow over the northern

Colorado Rockies driven by the influence of El Niño Southern Oscillation (ENSO) and Pacific Decadal Oscillation (PDO) (Anderson et al., 2016a; Barron and Anderson, 2011; Du et al., 2021, 2020; Liu et al., 2014; Steinman et al., 2014).

By ~1700 cal yr BP, a rapid shift to higher snowfall (relative to rain) and P-E occurred at Emerald and Pahrnagut lakes, which persisted at Emerald over the next several centuries. A similar shift to persistent cool and wet conditions at this time is also observed in the northern Rockies (Brown et al., 2021; Larsen et al., 2020; Stone et al., 2016). In contrast, Pahrnagut returned to slightly dry or average P-E, as did high elevations in the northern Colorado Rockies at Bison and Yellow Lakes. These geographic differences may present a precipitation pattern similar in complexity to those identified by more distant precipitation- $\delta^{18}\text{O}$  and P-E comparisons along the margin of western North America (Anderson et al., 2016a; Barron and Anderson, 2011; Steinman et al., 2014).

The MCA is characterized by a rapid shift to low P-E at Emerald Lake as large variations in snowpack occurred in northwest Colorado at Bison and Yellow, and no trend is evident from Great Basin records, east or west (Lund and Benson, 2018; Munroe et al., 2018). These results support observations by Metcalf et al. (2015) who found considerable variability in the monsoon region during the MCA, which may reflect transient upper level ridging (Hermann et al., 2018) and/or persistent El Niño or La Niña states which affected both snowpack and summer rains (Anderson, 2012; Hart et al., 2021). The ubiquitously cold and wet LIA pattern observed at all of the high elevation lakes (Emerald, Bison and Yellow) indicates high winter snowfall driven by jet stream positioning over the intermountain west region. The pattern persisted for multiple decades and was associated with wet conditions at low elevations (Pahrnagut, Stonehouse Meadow).

## **Conclusions**

Paleoclimate histories that include surface hydrologic response across elevation gradients provide a means understand natural variations in water supply and thereby better inform water management for the intermountain west. The new Emerald Lake record indicates that throughout the Holocene extreme dry periods with significant reductions in high elevation snowpack have occurred, which at the  $\sim 40^{\circ}\text{N}$  extended eastward to the Upper Colorado headwaters and westward to the Great Basin. Furthermore, with the growing collection of high-elevation isotope records we can now place specific changes in snowpack sub-regions of the Upper Colorado River basin, and corresponding water supply, over recent decades and centuries within several long-term contexts. Results indicate Holocene extremes in snowpack variations expand upon observations based on shorter contexts (Pederson et al., 2013; Routson et al., 2011). This study shows that Upper Colorado River basin snowpack has undergone high magnitude change on a range of timescales, and that similar variations should be assessed within a 21<sup>st</sup> century context with caution. Framing observed trends within a longer context of multiple centuries to millennia allows more confident identification of significant trends, which will be essential to recognize in terms of future impacts on water supply.

Evaluating the future prognosis for intermountain snowpack is instructed by considering the evidence presented in response to the introductory questions. First, the proxy results show consistent paleohydrologic variations at high and low elevations on millennial to multi-century timescales, within the chronological precision of the records. Consistent multi-decadal variations also appear to occur near simultaneously, particularly when snowfall variations during the past  $\sim 2500$  years dominated paleohydrologic trends, although chronological precision at these

timescales is currently insufficient for confident correlations. This finding validates paleohydrologic reconstructions from low elevation lakes and wetlands can be confidently understood to represent water source variations. Second, the results confirm that precipitation extremes in the Upper Colorado were commonly regional, which implies synoptic scale climate forcing mechanisms, and thereby a potential for predictability. However, varied sub-regional differences that resemble precipitation dipoles and time-transgressive patterns are suggested, with prominent examples within the expanded envelope of the ‘Late Holocene Dry Period’ proposed here. In conclusion, the Emerald Lake paleohydrologic record, located at the boundary of the three major sub-regions of the intermountain west, the Great Basin, Upper Colorado River and Colorado Plateau regions from, brings clearer focus to the range of precipitation patterns and associated atmospheric transitions that can be anticipated to affect regional water supply in the future. There remain numerous western mountain ranges incorporating Paleozoic to Neogene limestones with small landslide affected (or formed) lakes in alpine settings that have yet to be fully investigated (*e.g.*, Shapley et al., 2021). This study also provides a framework for future investigations of the paleoclimatic signals embedded in their lithology and carbonate isotope geochemistry.

## **Acknowledgements**

The USGS ScienceBase data release for this publication is ----- . This research is supported by the U.S. Geological Survey Land Change Science Program. We thank Andrea Brunelle, Jesse Morris, Doug and Jessica, who provided logistical support and field assistance that made this research possible. David Dettman at the University of Arizona and Million Hailemichael at Idaho State University provided carbonate and water isotope data; AMS radiocarbon ages were

provided by Jack Reed at the USGS Radiocarbon Laboratory and Chad Wolack at the Institute for Arctic Antarctic and Alpine Research (INSTAAR) at the University of Colorado Boulder. Alisa Mast at the USGS Colorado Water Science Center provided water chemistry data. We appreciate reviews by Paul Henne and 2 anonymous journal reviewers for their constructive criticisms and suggestions that served to significantly improve the manuscript. Any use of trade, firm, or product names is for descriptive purposes only and does not imply endorsement by the U.S. Government.

The Supplementary Material for this article can be found at <https://doi.org/----->.

## **References**